Geophysical Research Letters

RESEARCH LETTER
10.1029/2023GL102894

Anthropogenic Bromoform at the Extratropical Tropopause

Yue Jia[1,2], Josefine Hahn[3,4], Birgit Quack[3], Edward Jones[5], Meghan Brehon[1], and Susann Tegtmeier[1]

[1]Institute of Space and Atmospheric Studies, University of Saskatchewan, Saskatoon, SK, Canada, [2]Now at Cooperative Institute for Research in Environmental Sciences (CIRES), University of Colorado Boulder, Boulder, CO, USA, [3]GEOMAR Helmholtz Centre for Ocean Research Kiel, Kiel, Germany, [4]Now at Helmholtz-Zentrum Hereon GmbH, Institute of Coastal Environmental Chemistry, Geesthacht, Germany, [5]Department of Physical Geography, Utrecht University, Utrecht, The Netherlands

Key Points:

- A new $CHBr_3$ emission inventory based on natural and anthropogenic sources suggests that the latter account for 12%–28% of the global emissions
- In the NH, new anthropogenic estimates increase known natural $CHBr_3$ emissions by up to 70.5%, leading to higher atmospheric $CHBr_3$ levels
- At the NH extratropical tropopause, $CHBr_3$ is enhanced by 0.9 ppt Br due to anthropogenic sources thus doubling natural $CHBr_3$ abundances

Correspondence to:

S. Tegtmeier,
susann.tegtmeier@usask.ca

Citation:

Jia, Y., Hahn, J., Quack, B., Jones, E., Brehon, M., & Tegtmeier, S. (2023). Anthropogenic bromoform at the extratropical tropopause. *Geophysical Research Letters*, *50*, e2023GL102894. https://doi.org/10.1029/2023GL102894

Received 17 JAN 2023
Accepted 15 APR 2023

Abstract Bromoform ($CHBr_3$) contributes to stratospheric ozone depletion but is not regulated under the Montreal Protocol due to its short lifetime and large natural sources. Here, we show that anthropogenic sources contribute significantly to the amount of $CHBr_3$ transported into the Northern Hemisphere (NH) extratropical stratosphere. We present a new $CHBr_3$ emission inventory comprised of natural and anthropogenic sources, with the latter estimated from ship ballast, power plant cooling and desalination plant brine water. Including anthropogenic sources in the new inventory increases $CHBr_3$ emissions by up to 31.5% globally and 70.5% in the NH. In consequence, atmospheric $CHBr_3$ is also significantly higher, especially over the NH extratropics during boreal winter. Here anthropogenic sources enhance bromine at the tropopause by 0.9 ppt Br, thus doubling natural $CHBr_3$ abundances. For some latitudes, tropopause bromine increases by 2.4 ppt Br suggesting significant contributions of anthropogenic $CHBr_3$ to the NH lowermost stratosphere.

Plain Language Summary Halogen-containing compounds are emitted at the Earth's surface and transported into the stratosphere, where they contribute to the depletion of the ozone layer. Emissions of long-lived halogen compounds such as CFC-11 have been reduced following the implementation of the Montreal Protocol and its later adjustments. Emissions of short-lived halogen-containing compounds, on the other hand, are currently not regulated. Within this group, bromoform ($CHBr_3$) is one of the most abundant compounds and has been known to have mostly natural sources. In this study, we present a new data set of $CHBr_3$ emissions which includes anthropogenic sources from industrial water use. We show that these anthropogenic sources increase global $CHBr_3$ emissions by one-third. Our results also suggest that the anthropogenic emissions contribute significantly to the amount of $CHBr_3$ transported into the stratosphere over the Northern Hemisphere mid-latitudes.

1. Introduction

Bromocarbons with atmospheric lifetimes shorter than 6 months belong to the so-called very short-lived substances (VSLSs). These substances are significant sources of stratospheric bromine (Br) and contribute to chemical ozone depletion (Laube & Tegtmeier, 2022). Among the VSLSs, oceanic bromoform ($CHBr_3$) is the largest carrier of organic bromine to the atmosphere (Quack & Wallace, 2003). Several attempts have been made to estimate $CHBr_3$ emissions from marine sources. However, due to sparse measurements and missing process understanding, those estimates are subject to large uncertainties. There are two main approaches to derive $CHBr_3$ emission inventories, that is, the "bottom-up" approach (e.g., Quack & Wallace, 2003; Ziska et al., 2013) and the "top-down" approach (e.g., Liang et al., 2010; Ordóñez et al., 2012; Warwick et al., 2006). For the bottom-up approach, statistical gap filling is applied to observational surface seawater and air concentrations to derive gap-free maps of these quantities from which emissions of $CHBr_3$ are calculated. Top-down methods use global model simulations to constrain emission inventories so that they reproduce observed atmospheric concentrations. The global $CHBr_3$ source estimates span a range of 120–820 Gg Br/yr (e.g., Tables 1–8 in Carpenter et al., 2014) with the emission inventories based on top-down approaches typically being higher than those from bottom-up approaches.

Bromoform is largely produced by marine organisms such as macroalgae and phytoplankton (Carpenter & Liss, 2000; Gschwend et al., 1985) with elevated production in coastal and shelf waters. High oceanic concentrations in these regions can also result from anthropogenic sources (Boudjellaba et al., 2016) such as ballast water

(Liu et al., 2015; Maas et al., 2019), power plants (Maas et al., 2021; Yang, 2001), and desalination facilities (Agus et al., 2009), as disinfection of seawater in these industries produces large amounts of $CHBr_3$. Some of the difference in estimates of emissions derived from top-down and bottom-up approaches might be explained by anthropogenic inputs of organic bromine, which are usually insufficiently included in the latter (Maas et al., 2021).

Stratospheric injection of $CHBr_3$ and other brominated VSLSs occurs mostly via the tropical tropopause and current estimates suggest that this pathway contributes 5 ± 2 ppt Br to the stratosphere (Laube & Tegtmeier, 2022). Given their short lifetimes, mostly tropical VSLSs sources contribute to this injection pathway (Tegtmeier et al., 2015) and anthropogenic sources at mid-latitudes do not play a role (Maas et al., 2021). However, the situation is completely different for the extratropical lowermost stratosphere (the region between the tropopause and 380 K), where both tropical and extratropical sources contribute to trace gas abundances (e.g., Gettelman et al., 2011; Holton & Hakim, 2013). Three recent aircraft campaigns with the High Altitude and Long Range Research Aircraft (HALO) revealed relatively high $CHBr_3$ at the extratropical tropopause during boreal winter with a strong latitudinal gradient (Keber et al., 2020). This increase of $CHBr_3$ with latitude is partially related to the longer local lifetimes during winter. In addition, extratropical $CHBr_3$ emissions might also play a role. Model simulations based on bottom-up emission inventories without anthropogenic source terms have difficulties in reproducing observed $CHBr_3$ at extratropical latitudes highlighting the importance of the latitudinal distribution of the emissions (Keber et al., 2020; Maas et al., 2021). As bromine chemistry plays an important role for lowermost stratospheric ozone loss (Salawitch et al., 2005) with a relatively large radiative effect (Hossaini et al., 2015), the overall contributions of anthropogenic $CHBr_3$ sources need to be quantified for understanding and predicting long-term ozone changes.

In this paper, we present a new $CHBr_3$ emission inventory, which combines the bottom-up emission inventory from Ziska et al. (2013) with emissions estimated from anthropogenic sources. Here, we consider $CHBr_3$ emissions arising from the chemical treatment of water for: (a) use as ballast, (b) cooling thermoelectric power plants, and (c) freshwater production via desalination (Maas et al., 2019, 2021). Based on the new emission inventory (Jia et al., 2023), the Lagrangian dispersion model FLEXPART is used to simulate the $CHBr_3$ distribution in the extratropical lower stratosphere. The emission inventory and FLEXPART model are described in Section 2. In Section 3, we present the simulation results and the comparisons with observational data. Summary and conclusions are given in Section 4.

2. Data and Methodology

2.1. Emission Inventory

The $CHBr_3$ emission inventory presented in this study is a combination of bottom-up emissions from Ziska et al. (2013) (updated in Fiehn et al. (2018); hereafter Ziska emissions) and anthropogenic emissions from ballast water (Maas et al., 2019), power plant cooling water (Maas et al., 2021), and effluents from desalination plants. Taking into account the physical and biogeochemical characteristics of the ocean and atmosphere, Ziska et al. (2013) extrapolated available surface ocean and atmosphere measurement to derive a regularly gridded global $CHBr_3$ emission inventory. Due to sparse measurements, the Ziska emission inventory is known to underestimate $CHBr_3$ emissions in coastal regions, where anthropogenic sources dominate, and mainly represents the natural sources of $CHBr_3$.

Anthropogenic $CHBr_3$ emissions are derived by combining available $CHBr_3$ measurements in different types of wastewaters (Grote et al., 2022) with respective estimates of industrial water use. In a first step, concentrations of anthropogenic $CHBr_3$ in water are derived. Therefore, ship ballast water estimates inferred from world port rankings are combined with $CHBr_3$ concentrations observed in ballast water (Maas et al., 2019); coastal cooling-water volumes derived from global power plant databases (Davis et al., 2012) are combined with $CHBr_3$ measured in power plant effluents (Maas et al., 2021); and country specific desalination plant brine data separated into sea- and brackish water (Jones et al., 2019) are combined with $CHBr_3$ brine measurements. In a second step, all anthropogenic sources are added together and scaled into low and high emission inventories based on the uncertainty range of $CHBr_3$ concentrations within the effluents.

In a final step, the anthropogenic $CHBr_3$ emissions are calculated following the general flux equation at the air-sea interface:

Table 1
$CHBr_3$ Prescribed Lifetimes Based on Carpenter et al. (2014)

$CHBr_3$	Tropics (25°S–25°N)		Extratropics (25°N–90°N, 25°S–90°S)							
Lifetimes (days)	<3 km	>3 km	<3 km				>3 km			
			Summer	Fall	Winter	Spring	Summer	Fall	Winter	Spring
	15	17	14	35	86	20	17	44	88	29

Note. The seasons (summer, fall, winter, and spring) listed in the table correspond to JJA, SON, DJF, and MAM in the Northern Hemisphere. And DJF, MAM, JJA, and SON in the Southern Hemisphere, respectively.

$$\text{Flux} = \left(C_w - C_{\text{eq}}\right) \times k \tag{1}$$

Here, flux is positive when it is directed from the ocean to the atmosphere. C_w is the actual concentration in the surface mixed layer, and

$$C_{\text{eq}} = C_{\text{air}} \times H^{-1}_{\text{CHBr}_3} \tag{2}$$

is the theoretical equilibrium concentration at the sea surface calculated from the atmospheric mixing ratio and Henry's law constant of $CHBr_3$. The gas transfer velocity k mainly depends on the surface wind speed and temperature and is calculated following Nightingale et al. (2000). Wind velocities at 10 m height are taken from the ERA-Interim atmospheric data product.

For the new inventory, the Ziska and anthropogenic $CHBr_3$ emissions are merged by taking the maximum value of the two emission estimates in each grid cell (1° × 1°). The maximum value, and not the sum, is used here to avoid overestimates of $CHBr_3$ in coastal regions. Based on the existing range of anthropogenic emission estimates, two new $CHBr_3$ emission inventories are derived, which we refer to as Mixed_Low and Mixed_High.

2.2. FLEXPART Simulations for 2016–2017

To simulate the atmospheric distribution and transport of $CHBr_3$, we performed global simulations in the forward mode for 2016 and 2017 for each emission inventory with 2-month spin-up using the Lagrangian particle dispersion model FLEXPART (Pisso et al., 2019). FLEXPART has been validated extensively by previous comparisons with measurements (e.g., Stohl & Trickl, 1999; Stohl et al., 1998). Three-hourly meteorological fields from the European Center for Medium-Range Weather Forecasts (ECMWF) reanalysis product ERA-Interim (Dee et al., 2011) with a horizontal resolution of 1° × 1° and 60 vertical model levels, are used to drive the model. Chemical or radioactive decay of $CHBr_3$ is accounted for by reducing the tracer mass in air parcels according to prescribed lifetimes. In this study, we employ a version of FLEXPART tuned to account for latitude-, altitude-, and time-dependent lifetimes of $CHBr_3$. The lifetimes of $CHBr_3$ are prescribed as listed in Table 1, with ∼17 days for the tropics and extratropical summer and ∼90 days for the extratropical winter (Carpenter et al., 2014).

We conducted additional runs to further analyze the impact of the seasonal and latitudinal lifetime variations. Our simulations indicate that $CHBr_3$ mixing ratios at the tropical and extratropical tropopause in the summer hemisphere are most sensitive to changes in lifetimes. Specifically, a 20% increase (decrease) in lifetimes results in ∼25% increase (decrease) in the mixing ratios at the tropical and summer extratropical tropopause. At the winter extratropical tropopause, this number is approximately 17%. In contrast, the surface mixing ratios show less sensitivity to changes in lifetimes, with $CHBr_3$ changing by less than 10% in the winter extratropics when lifetimes are varied by 20%.

3. Results

3.1. Anthropogenic $CHBr_3$ Emissions

The anthropogenic $CHBr_3$ emissions are centered at the coastal regions of the Northern Hemisphere (NH) extratropics (Figure 1). The majority of the emissions are found in developed regions and areas of emerging economies such as Europe, North America, East Asia, and South Asia and are distributed around centers of industry and

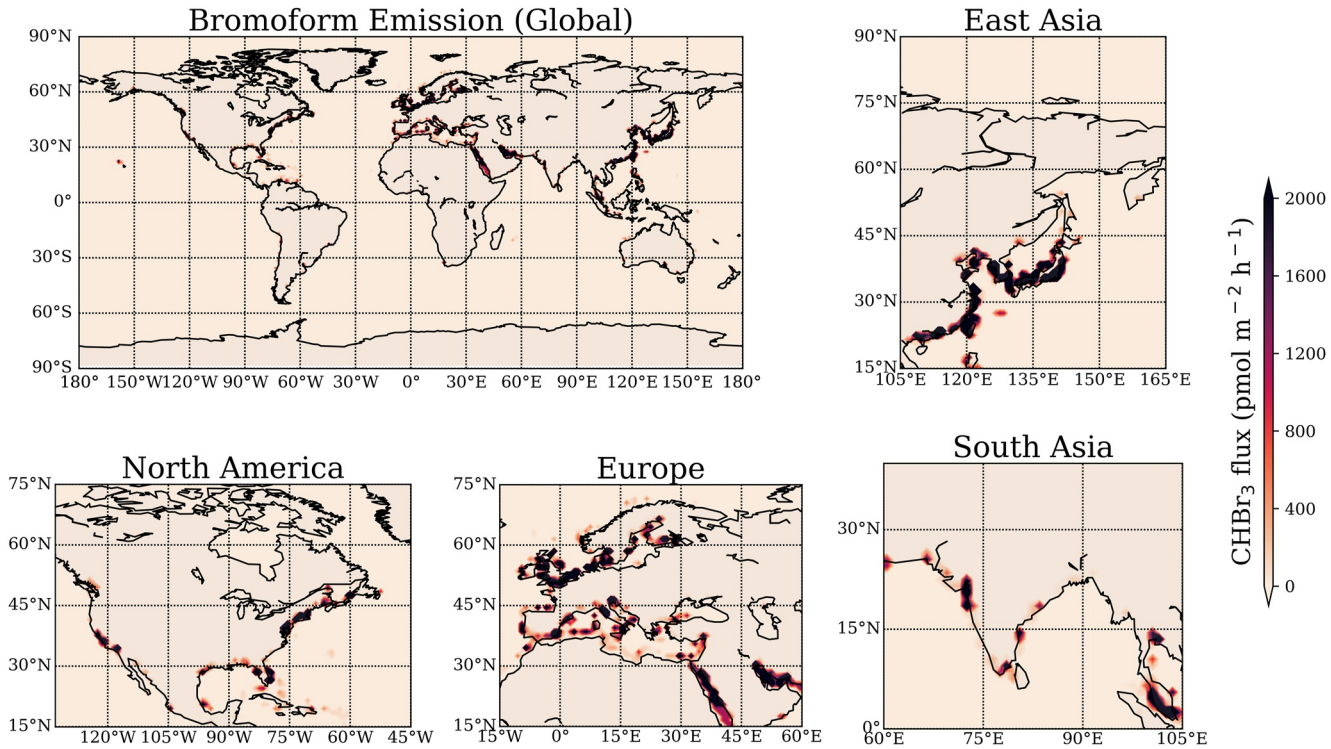

Figure 1. The lower-end estimates of anthropogenic $CHBr_3$ emissions from ship ballast water, cooling water from thermoelectric powerplants and desalination plants.

energy production. Globally, anthropogenic emissions contribute 18.6–50.0 Gg Br/yr, while bottom-up Ziska emissions total 135.8 Gg Br/yr. Our estimate of the anthropogenic $CHBr_3$ emissions agrees well with a previous estimate of 28 Gg Br/yr, which was derived as a global mean value without a breakdown into regional estimates (Quack & Wallace, 2003). In total, our new combined inventory suggests $CHBr_3$ emissions of between 149.5 Gg Br/yr (Mixed_Low) and 178.6 Gg Br/yr (Mixed_High). Globally, the anthropogenic emissions in the new inventory lead to a 10.1% and 31.5% increase compared to natural emissions for the low and high anthropogenic inventories, respectively. In the NH, anthropogenic sources increase emissions by up to 70.5%. The largest fraction of the anthropogenic emissions stems from global power plants (10.3%–25.9% of total $CHBr_3$ emissions), while desalination (1.8%–2.1%) and ship ballast water (0.1%–0.3%) provide only small contributions.

3.2. Vertical Distribution of $CHBr_3$

The vertical distribution of $CHBr_3$ is influenced by emission magnitudes, lifetimes and transport processes (Jia et al., 2019, 2022). The emission magnitudes strongly determine the mixing ratios near the surface. In the free troposphere and stratosphere, high $CHBr_3$ mixing ratios are expected to be found in the regions with longer lifetimes (e.g., extratropics of winter hemisphere), and in regions with strong convection (e.g., Liang et al., 2014; Tegtmeier et al., 2012). Based on the new combined emission inventory, we simulate the atmospheric $CHBr_3$ distribution and compare the results with those based on Ziska emissions only. The profiles of $CHBr_3$ mixing ratios averaged over different regions during boreal winter are shown in Figure 2. Anthropogenic sources contribute up to 50% to $CHBr_3$ abundances in the lower atmosphere, in particular in regions of high energy production (Figures 2a–2c). The $CHBr_3$ mixing ratios below 5 km over East Asia, North America, and Europe are generally higher than those over South Asia for all emission inventories because of the much longer lifetimes at higher latitudes during boreal winter. Earlier simulations of enhanced $CHBr_3$ due to anthropogenic production have already shown excellent agreement with boundary layer and free tropospheric aircraft observations over South Korea and adjacent seas (Maas et al., 2021).

All regions show a decrease of $CHBr_3$ between the boundary layer and the free troposphere with the anthropogenic contributions dropping to ~20%–40%. Similar to the lower atmosphere, free tropospheric $CHBr_3$ profiles over East Asia, North America, and Europe show a higher anthropogenic fraction than profiles over South Asia.

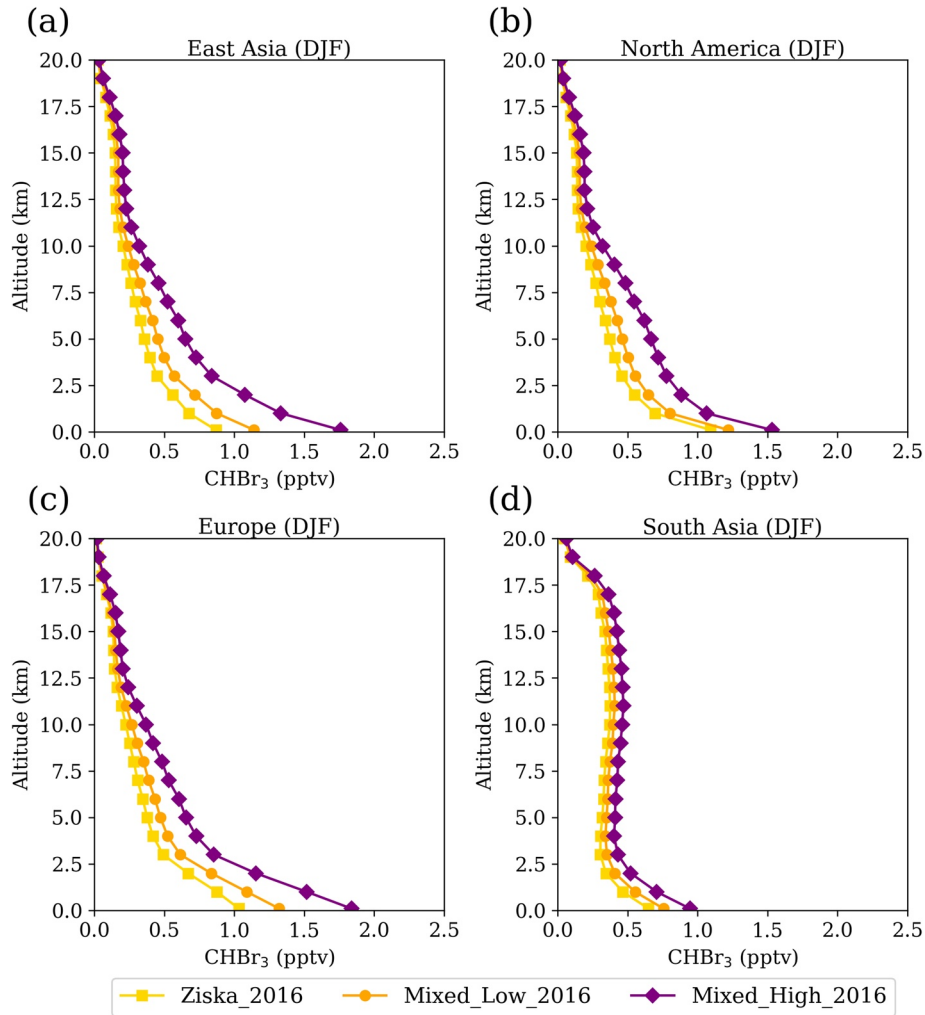

Figure 2. Simulated $CHBr_3$ profiles averaged over (a) East Asia, (b) North America, (c) Europe, and (d) South Asia in 2015–2016 boreal winter based on three different emission inventories. The regions are the same as shown in Figure 1.

This is roughly consistent with the emission distribution (Figure 1), suggesting the importance of natural and anthropogenic source locations in determining the $CHBr_3$ distribution in the free troposphere. Another drop in the $CHBr_3$ profiles occurs between the free troposphere and the UTLS, with the contribution of anthropogenic $CHBr_3$ becoming very small well above the tropopause where tropical airmasses impact the composition. It is noteworthy that the altitude of the $CHBr_3$ drop in South Asia is higher than for the other regions, suggesting the impact of stronger high-reaching convection. As the variations of prescribed lifetimes with altitude in our simulations are not significant, the vertical distribution of $CHBr_3$ is mainly impacted by transport processes.

3.3. Distribution of $CHBr_3$ at the Tropopause

The simulated $CHBr_3$ mixing ratios are interpolated to the dynamical tropopause height (two potential vorticity units, pvu), which are obtained from ERA-Interim (Figure 3). In the NH extratropics, $CHBr_3$ mixing ratios based on Mixed_Low and Mixed_High emissions are significantly larger than those based on Ziska emissions, especially during boreal winter, highlighting the importance of extratropical anthropogenic sources. The impact of anthropogenic $CHBr_3$ in this region is further enhanced by the longer $CHBr_3$ lifetimes during boreal winter, which contribute to the latitudinal gradients of $CHBr_3$ reported for the tropopause (Keber et al., 2020). In the Southern Hemisphere (SH) extratropics, the longer lifetimes during boreal winter also result in a higher $CHBr_3$ abundance at the tropopause (~0.5 ppt, zonal average), however these are not as pronounced as in the NH (~0.8 ppt, zonal average) and are independent of the anthropogenic emissions.

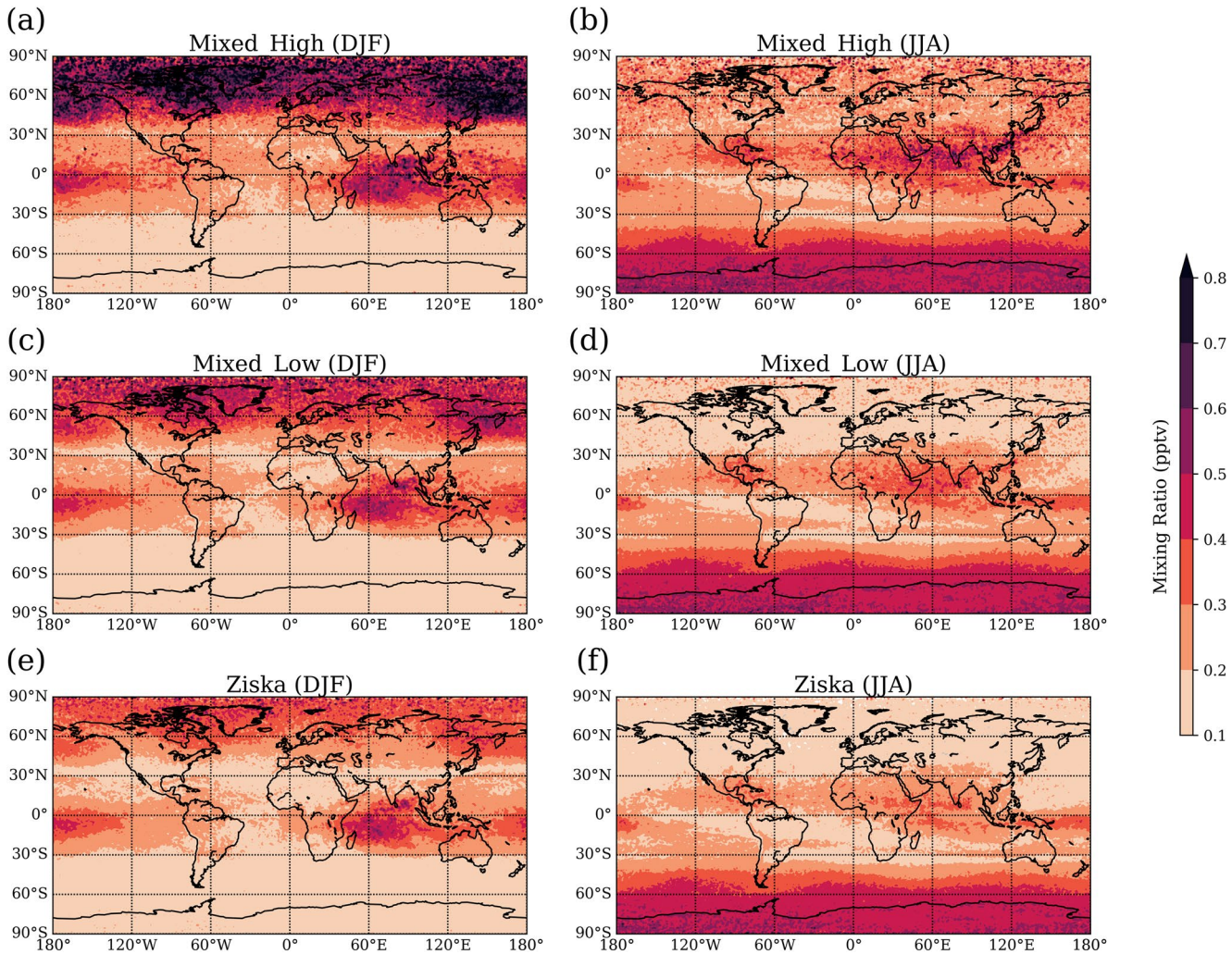

Figure 3. Latitude-longitude cross-sections of $CHBr_3$ mixing ratio at the dynamical tropopause (2 pvu) from FLEXPART simulations (2016) based on mixed emission with a high anthropogenic emission rate (a), (b), and a low anthropogenic emission rate (c), (d), as well as based on Ziska emissions only (e), (f).

In the tropics, relatively high $CHBr_3$ mixing ratios are found over the tropical Indian Ocean, the Maritime Continent, and Western Pacific for all three estimates of emission, demonstrating that these regions serve as efficient pathways for the transport of $CHBr_3$ into the stratosphere (Fernandez et al., 2014; Liang et al., 2014; Tegtmeier et al., 2012). However, the tropical $CHBr_3$ peaks in boreal summer are weaker than those in boreal winter, illustrating that NH extratropical sources and their boundary layer transport into the tropics can modulate the distribution of $CHBr_3$ at the tropical tropopause (Maas et al., 2021).

In order to analyze the impact of anthropogenic emissions on $CHBr_3$ reaching the extratropical tropopause, we examine a case study of $CHBr_3$ over the North America, Atlantic and Europe longitudinal range (180° W–30° E) so that our simulations can be compared with the observational data shown in Jesswein et al. (2022). We simulate $CHBr_3$ at the extratropical dynamical tropopause based on the Ziska and the two mixed emission inventories, with the latter two explicitly taking anthropogenic sources into account. Figure 4 shows the latitudinal cross sections of simulated $CHBr_3$ mixing ratios at the dynamical tropopause binned by latitude for December 2015 to February 2016 (Figure 4a) and September–November 2017 (Figure 4b) together with the observational data from Jesswein et al. (2022). The simulation period was chosen to ensure overlap with the observational data, which is to a large degree based on the three campaigns PGS (December 2015-March 2016), WISE_TACTS (September–October 2017) and ATom-3 (September–October 2017).

Extratropical $CHBr_3$ that includes anthropogenic emissions increases by 40%–90% for the 2015–2016 boreal winter (Figures 4a) and 50%–106% for the 2017 fall (Figure 4b), when compared to estimates based on Ziska

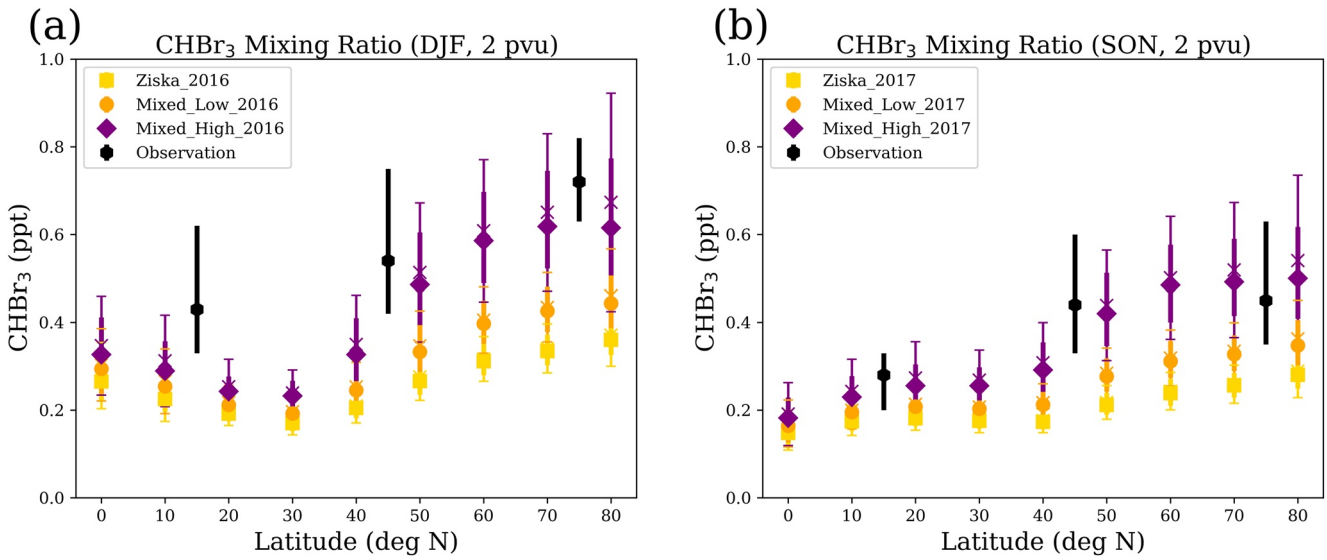

Figure 4. Simulated $CHBr_3$ mixing ratios at the dynamical tropopause averaged over (a) December 2015 to February 2016, 180°W–30°E, and (b) September–November 2017, 180°W–30°E. The reference $CHBr_3$ mixing ratios within 10K below the dynamical tropopause from Jesswein et al. (2022) are also presented. The thick markers represent the medians and the thick vertical bars show the range between 25th and 75th percentiles. The crosses indicate the means, and the thin vertical bars represent the standard deviations.

emissions only. For all emission estimates, simulated $CHBr_3$ at the tropopause increases with latitude north of 30° N as also reported by aircraft observations (e.g., Keber et al., 2020). This latitudinal increase is best reproduced by the simulations taking into account high anthropogenic emissions. During boreal winter, simulated $CHBr_3$ increases from 0.49 ppt at 50° N to 0.618 ppt at 70° N showing very good agreement with the observations (0.54 ppt in the NH mid-latitudes and 0.72 in the NH high latitudes). During boreal fall, simulated $CHBr_3$ based on high anthropogenic emissions increases from 0.42 ppt around 50° N to 0.49 ppt around 70° N, again consistent with the observations (0.44 ppt in the NH mid-latitudes and 0.45 in the NH high latitudes). Overall, our simulations that account for the high anthropogenic emissions show very good agreement with the absolute values and latitudinal gradients captured by the aircraft observations.

4. Summary and Conclusions

$CHBr_3$ emissions contribute to the stratospheric halogen loading and, thus, to ozone depletion. While current oceanic emission inventories show large variations, all inventories assume natural oceanic production as the main $CHBr_3$ source.

In this study, we present a new $CHBr_3$ emission inventory based on natural oceanic emissions (Ziska et al., 2013) and anthropogenic emissions estimated from ship ballast water treatment, cooling water of thermoelectric power plants, and effluents from desalination plants (Maas et al., 2019, 2021). Uncertainties in the anthropogenic emission estimates are relatively large due to substantial variations in $CHBr_3$ observed in chemically treated water, and therefore two new emission inventories (Mixed_Low and Mixed_High) have been derived. The anthropogenic $CHBr_3$ emissions are centered at the coastal regions of the NH extratropics distributed around the centers of industry and energy production in Europe, North America, East Asia, and South Asia. Globally, the anthropogenic emissions in the new inventory lead to a 10.1% and 31.5% increase compared to natural emissions for the low and high anthropogenic emission inventories, respectively. For the NH, where the majority of the industrialized regions are located, anthropogenic $CHBr_3$ sources are more important causing an emission increase of 22.7% and 70.5%.

When including the new anthropogenic emissions, the model-derived atmospheric distribution of $CHBr_3$ increases strongly over the NH extratropics, especially during boreal winter when $CHBr_3$ shows a longer lifetime. Anthropogenic sources lead to an increase of $CHBr_3$ at the dynamical tropopause of the NH extratropics by 0.3 and 0.13 ppt during boreal winter and summer, respectively, which doubles the mixing ratios due to

natural emissions. Such enhanced $CHBr_3$ values have also been reported by recent aircraft observations (Keber et al., 2020), in accordance with our estimates. The observed latitudinal gradients of $CHBr_3$ mixing ratios at the NH tropopause are best reproduced if high anthropogenic emissions are accounted for. Our simulations suggest that anthropogenic activities can enhance VSLSs at the NH extratropical tropopause by up to 0.8 ppt $CHBr_3$ (zonal average), resulting in a total of up to 1.2 ppt $CHBr_3$ (zonal average), which is of relevance for the amount of bromine transported into the lowermost stratosphere.

Data Availability Statement

The emission inventory and FLEXPART simulations are available from Jia et al. (2023). FLEXPART codes are available from https://www.flexpart.eu/. ERA-Interim reanalysis data are available from https://apps.ecmwf.int/datasets/data/interim-full-daily/levtype=sfc/.

Acknowledgments
The authors would like to thank the European Centre for Medium-Range Weather Forecasts (ECMWF) for the ERA-Interim reanalysis data and the FLEXPART development team for the Lagrangian particle dispersion model used in this publication. This research has been enabled by the NSERC Discovery Grant RGPIN-2020-06292.

References

Agus, E., Voutchkov, N., & Sedlak, D. L. (2009). Disinfection by-products and their potential impact on the quality of water produced by desalination systems: A literature review. *Desalination*, *237*(1), 214–237. https://doi.org/10.1016/j.desal.2007.11.059

Boudjellaba, D., Dron, J., Revenko, G., Démelas, C., & Boudenne, J. L. (2016). Chlorination by-product concentration levels in seawater and fish of an industrialised bay (Gulf of Fos, France) exposed to multiple chlorinated effluents. *Science of the Total Environment*, *541*, 391–399. https://doi.org/10.1016/j.scitotenv.2015.09.046

Carpenter, L. J., & Liss, P. S. (2000). On temperate sources of bromoform and other reactive organic bromine gases. *Journal of Geophysical Research*, *105*(D16), 20539–20547. 10.1029/2000JD900242

Carpenter, L. J., Reimann, S., Burkholder, J. B., Clerbaux, C., Hall, B. D., & Hossaini, R. (2014). Ozone-depleting substances (ODSs) and other gases of interest to the Montreal Protocol. In A. Engel & S. A. Montzka (Eds.), *Scientific assessment of ozone depletion: 2014. Global ozone research and Monitoring Project-Report A*. World Meteorological Organization.

Davis, C., Chmieliauskas, A., Dijkema, G., & Nikolic, I. (2012). *Enipedia, energy and industry group Faculty of Technology Policy and Management (Technical report)*. TU Delft. Retrieved from: http://enipedia.tudelft.nl

Dee, D. P., Uppala, S. M., Simmons, A. J., Berrisford, P., Poli, P., Kobayashi, S., et al. (2011). The ERA-interim reanalysis: Configuration and performance of the data assimilation system. *Quarterly Journal of the Royal Meteorological Society*, *137*(656), 553–597. 10.1002/qj.828

Fernandez, R. P., Salawitch, R. J., Kinnison, D. E., Lamarque, J. F., & Saiz-Lopez, A. (2014). Bromine partitioning in the tropical tropopause layer: Implications for stratospheric injection. *Atmospheric Chemistry and Physics*, *14*(24), 13391–13410. https://doi.org/10.5194/acp-14-13391-2014

Fiehn, A., Quack, B., Stemmler, I., Ziska, F., & Krüger, K. (2018). Importance of seasonally resolved oceanic emissions for bromoform delivery from the tropical Indian Ocean and west Pacific to the stratosphere. *Atmospheric Chemistry and Physics*, *18*(16), 11973–11990. https://acp.copernicus.org/articles/18/11973/2018/

Gettelman, A., Hoor, P., Pan, L. L., Randel, W. J., Hegglin, M. I., & Birner, T. (2011). The extratropical upper troposphere and lower stratosphere. *Reviews of Geophysics*, *49*(3), RG3003. https://doi.org/10.1029/2011RG000355

Grote, M., Boudenne, J.-L., Croué, J.-P., Escher, B. I., von Gunten, U., Hahn, J., et al. (2022). Inputs of disinfection by-products to the marine environment from various industrial activities: Comparison to natural production. *Water Research*, *217*, 118383. https://doi.org/10.1016/j.watres.2022.118383

Gschwend, P. M., MacFarlane, J. K., & Newman, K. A. (1985). Volatile Halogenated organic compounds released to seawater from temperate marine macroalgae. *Science*, *227*(4690), 1033–1035. https://www.science.org/doi/abs/10.1126/science.227.4690.1033

Holton, J. R., & Hakim, G. J. (2013). *An Introduction to dynamic meteorology* (5th ed., p. 522). Academic Press. 10.1016/C2009-0-63394-8

Hossaini, R., Chipperfield, M. P., Montzka, S. A., Rap, A., Dhomse, S., & Feng, W. (2015). Efficiency of short-lived halogens at influencing climate through depletion of stratospheric ozone. *Nature Geoscience*, *8*(3), 186–190. https://doi.org/10.1038/ngeo2363

Jesswein, M., Fernandez, R. P., Berná, L., Saiz-Lopez, A., Grooß, J. U., Hossaini, R., et al. (2022). Global seasonal distribution of CH_2Br_2 and $CHBr_3$ in the upper troposphere and lower stratosphere. *Atmospheric Chemistry and Physics*, *22*(22), 15049–15070. https://doi.org/10.5194/acp-22-15049-2022

Jia, Y., Hahn, J., Quack, B., Jones, E., & Tegtmeier, S. (2023). Anthropogenic bromoform at the extratropical tropopause [dataset]. Zenodo. https://doi.org/10.5281/zenodo.7535206

Jia, Y., Quack, B., Kinley, R. D., Pisso, I., & Tegtmeier, S. (2022). Potential environmental impact of bromoform from Asparagopsis farming in Australia. *Atmospheric Chemistry and Physics*, *22*(11), 7631–7646. https://doi.org/10.5194/acp-22-7631-2022

Jia, Y., Tegtmeier, S., Atlas, E., & Quack, B. (2019). How marine emissions of bromoform impact the remote atmosphere. *Atmospheric Chemistry and Physics*, *19*(17), 11089–11103. https://doi.org/10.5194/acp-19-11089-2019

Jones, E., Qadir, M., van Vliet, M. T. H., Smakhtin, V., & Kang, S.-m. (2019). The state of desalination and brine production: A global outlook. *Science of the Total Environment*, *657*, 1343–1356. https://doi.org/10.1016/j.scitotenv.2018.12.076

Keber, T., Bönisch, H., Hartick, C., Hauck, M., Lefrancois, F., Obersteiner, F., et al. (2020). Bromine from short-lived source gases in the extratropical northern hemispheric upper troposphere and lower stratosphere (UTLS). *Atmospheric Chemistry and Physics*, *20*(7), 4105–4132. https://doi.org/10.5194/acp-20-4105-2020

Laube, J. C., & Tegtmeier, S. (2022). *Update on ozone-depleting substances (ODSs) and other gases of interest to the Montreal Protocol, Chapter 1 in Scientific Assessment of Ozone Depletion: 2022* (p. 509). GAW Report No. 278. Geneva: WMO.

Liang, Q., Atlas, E., Blake, D., Dorf, M., Pfeilsticker, K., & Schauffler, S. (2014). Convective transport of very short lived bromocarbons to the stratosphere. *Atmospheric Chemistry and Physics*, *14*(11), 5781–5792. https://doi.org/10.5194/acp-14-5781-2014

Liang, Q., Stolarski, R. S., Kawa, S. R., Nielsen, J. E., Douglass, A. R., Rodriguez, J. M., et al. (2010). Finding the missing stratospheric Br_y: A global modeling study of $CHBr_3$ and CH_2Br_2. *Atmospheric Chemistry and Physics*, *10*(5), 2269–2286. https://doi.org/10.5194/acp-10-2269-2010

Liu, Z., Wang, X., Luo, Z., Huo, M., Wu, J., Huo, H., & Yang, W. (2015). Removing of disinfection by-product precursors from surface water by using magnetic graphene oxide. *PLoS One*, *10*(12), e0143819. https://doi.org/10.1371/journal.pone.0143819

Maas, J., Tegtmeier, S., Jia, Y., Quack, B., Durgadoo, J. V., & Biastoch, A. (2021). Simulations of anthropogenic bromoform indicate high emissions at the coast of East Asia. *Atmospheric Chemistry and Physics*, *21*(5), 4103–4121. https://doi.org/10.5194/acp-21-4103-2021

Maas, J., Tegtmeier, S., Quack, B., Biastoch, A., Durgadoo, J. V., Rühs, S., et al. (2019). Simulating the spread of disinfection by-products and anthropogenic bromoform emissions from ballast water discharge in Southeast Asia. *Ocean Science*, *15*(4), 891–904. https://doi.org/10.5194/os-15-891-2019

Nightingale, D., Malin, G., Law, C. S., Watson, A. J., Liss, P. S., Liddicoat, M. I., et al. (2000). In situ evaluation of air-sea gas exchange parameterizations using novel conservative and volatile tracers. *Global Biogeochemical Cycles*, *14*(1), 373–387. https://doi.org/10.1029/1999gb900091

Ordóñez, C., Lamarque, J. F., Tilmes, S., Kinnison, D. E., Atlas, E. L., Blake, D. R., et al. (2012). Bromine and iodine chemistry in a global chemistry-climate model: Description and evaluation of very short-lived oceanic sources. *Atmospheric Chemistry and Physics*, *12*(3), 1423–1447. https://doi.org/10.5194/acp-12-1423-2012

Pisso, I., Sollum, E., Grythe, H., Kristiansen, N. I., Cassiani, M., Eckhardt, S., et al. (2019). The Lagrangian particle dispersion model FLEXPART version 10.4. *Geoscientific Model Development*, *12*(12), 4955–4997. https://doi.org/10.5194/gmd-12-4955-2019

Quack, B., & Wallace, D. W. R. (2003). Air-sea flux of bromoform: Controls, rates, and implications. *Global Biogeochemical Cycles*, *17*(1). https://doi.org/10.1029/2002GB001890

Salawitch, R. J., Weisenstein, D. K., Kovalenko, L. J., Sioris, C. E., Wennberg, P. O., Chance, K., et al. (2005). Sensitivity of ozone to bromine in the lower stratosphere. *Geophysical Research Letters*, *32*(5), L05811. https://doi.org/10.1029/2004GL021504

Stohl, A., Hittenberger, M., & Wotawa, G. (1998). Validation of the Lagrangian particle dispersion model FLEXPART against largescale tracer experiment data. *Atmospheric Environment*, *32*(24), 4245–4264. https://doi.org/10.1016/S1352-2310(98)00184-8

Stohl, A., & Trickl, T. (1999). A textbook example of long-range transport: Simultaneous observation of ozone maxima of stratospheric and North American origin in the free troposphere over Europe. *Journal of Geophysical Research*, *104*(D23), 30445–30462. https://doi.org/10.1029/1999JD900803

Tegtmeier, S., Krüger, K., Quack, B., Atlas, E. L., Pisso, I., Stohl, A., & Yang, X. (2012). Emission and transport of bromocarbons: From the west Pacific ocean into the stratosphere. *Atmospheric Chemistry and Physics*, *12*(22), 10633–10648. https://doi.org/10.5194/acp-12-10633-2012

Tegtmeier, S., Ziska, F., Pisso, I., Quack, B., Velders, G. J. M., Yang, X., & Krüger, K. (2015). Oceanic bromoform emissions weighted by their ozone depletion potential. *Atmospheric Chemistry and Physics*, *15*(23), 13647–13663. https://doi.org/10.5194/acp-15-13647-2015

Warwick, N. J., Pyle, J. A., Carver, G. D., Yang, X., Savage, N. H., O'Connor, F. M., & Cox, R. A. (2006). Global modeling of biogenic bromocarbons. *Journal of Geophysical Research*, *111*(D24), D24305.

Yang, S. J. (2001). Bromoform in the effluents of a nuclear power plant: A potential tracer of coastal water masses. *Hydrobiologia*, *464*(1), 99–105. https://doi.org/10.1023/A:1013922731434

Ziska, F., Quack, B., Abrahamsson, K., Archer, S. D., Atlas, E., Bell, T., et al. (2013). Global sea-to-air flux climatology for bromoform, dibromomethane and methyl iodide. *Atmospheric Chemistry and Physics*, *13*(17), 8915–8934. https://doi.org/10.5194/acp-13-8915-2013